REPRINT

ChemistrySelect

Full Papers
doi.org/10.1002/slct.202002161

Chemistry
Europe
European Chemical
Societies Publishing

■ Materials Science inc. Nanomaterials & Polymers

Linear versus Branched Peptide with Same Amino Acid Sequence for Legumain-Targeting in Macrophages: Targeting Efficiency and Bioimaging Potential

Jayasree S. Kanathasan,[a] Diivananthan Gunasagaram,[a] Shafi Ullah Khan,[b]
Uma D. Palanisamy,[c] Ammu Kutty Radhakrishnan,[c] Nafees Ahemad,[b] and
Varghese Swamy*[a]

The relative legumain-targeting efficiency of a Y-shaped peptide and a linear peptide with the same amino acid sequence was investigated using in vitro experiments and computer simulations. Flow cytometry and fluorescence microscopy of cell types with varying levels of legumain expression (RAW 264.7, 4T1, MCF 10 A, MCF 7 and MDA MB 231) revealed that the linear peptide has a higher legumain binding efficiency in legumain-active cells compared to the Y-shaped peptide. Peptide-protein docking simulations showed that the more stable linear peptide binds at the active site of legumain, whereas the Y-shaped peptide binds at a different site. The Y-shaped peptide has its asparaginyl binding site (-Asn-) coiled into an α-helix form, and this reduces access to legumain binding. The linear peptide conjugated to fluorescent carbon dots (CDs) displayed enhanced binding efficiency towards legumain. The peptide-CDs conjugate nanoparticles are stable under pH, temperature, and medium composition conditions similar to that may be expected in tumor environments, suggesting their high potential as a bioimaging agent.

A range of targeting ligands have been employed in nanoparticle based theranostic formulations intended for treatment of cancer and other diseases.[1] In the case of cancer, the ligands are expected to selectively localize the nanoparticle formulations at tumor sites through specific interactions with cell–surface receptors or other biomolecules in tumor cells or tumor microenvironments, within the "active-targeting" strategy.[2] Among the commonly investigated ligands are monoclonal antibodies, polymers, nucleic acids, small molecules, carbohydrates, peptides, aptamers, and proteins.[1] Peptides have recently gained much attention as key ligand materials for nanoparticle-based drug delivery and bioimaging.[3] Peptide based formulations such as cilengitide and angiopep-2[4] are already in use for treating various diseases. The intrinsic advantages of nanoparticles, namely, tailorable size, shape, and surface charge facilitate multifunctionality, drug loading capability, enhanced retention and circulation, and effective accumulation at the desired site.[5] Surface functionalization of nanoparticles with a suitable peptide can lead to further enhancements and modifications of these nanoparticle advantages.

Peptides have several advantages as ligand materials. Owing to their relatively small size, peptides form compact nanoparticle coatings while maintaining the hydrodynamic diameter of the nanoparticle-peptide conjugate within limits. The specific properties of the peptide coating can be used to regulate the physical stability and circulation of the nanoparticles. Peptides are low cost materials, easily produced via solid-phase synthesis and functionalized using simple conjugation protocols. They offer the possibilities of lower immunogenicity, increased stability of presentation, increased diffusion and tissue penetration, and reduced binding to physiological biomolecules when compared to full length proteins[3] The interactions of the peptide with biomolecules in the host can either trigger macrophage recognition, phagocytosis and rapid clearance, or limit the immunological response and thus prolong circulation to ensure efficient accumulation in the desired tissue.[3d] Peptides can thus facilitate nanoparticle localization or penetration of cancer cell or tumor and drive imaging, detection and therapy.

Various types of peptide have been investigated using in vitro and in vivo techniques for their efficacies as nanomedical agents.[3] Factors including length, natural or unnatural amino acids present, geometry (linear, branched, or cyclic), pH-sensitivity, and interactions with biomolecules such as enzymes determine their physical and biological stability and therapeutic or diagnostic efficacies.[3] Peptides with 10–15 amino acids have been suggested in the past as ideal for nanomedicine, for smaller peptides with less than 5 amino acids may degrade in biological environments. However, longer cell-penetrating

[a] Dr. J. S. Kanathasan, D. Gunasagaram, Dr. V. Swamy
Mechanical Engineering Discipline, School of Engineering, Monash University Malaysia, Jalan Lagoon Selatan, Bandar Sunway, 47500 Selangor, Malaysia
E-mail: varghese.swamy@monash.edu
[b] S. U. Khan, Dr. N. Ahemad
School of Pharmacy, Monash University Malaysia, Jalan Lagoon Selatan, Bandar Sunway, 47500 Selangor, Malaysia
[c] Dr. U. D. Palanisamy, Prof. A. K. Radhakrishnan
Jeffrey Cheah School of Medicine and Health Sciences, Monash University Malaysia, Jalan Lagoon Selatan, Bandar Sunway, 47500 Selangor, Malaysia

peptides, with up to 30 amino acids, have been successfully used.[6] Structurally, linear peptides with 2–10 amino acids are more flexible in aqueous solution while those with up to 20 amino acids can develop secondary α-helices and β-strands.[7] The longer peptides may undergo conformational changes in the secondary structure upon binding to a receptor, potentially influenced by hydrogen bonds, and can lead to higher binding affinity.[8] Cyclized peptides have a propensity to develop β-turns which can contribute to greater binding efficiency. Also, the fixed geometry and improved cell penetrating ability of cyclized peptides can confer better targeting efficiency compared to linear peptides; however, depending on the amino acid sequences in the peptide, the opposite case is also possible.[9] Other than cyclization, peptides can also be designed as Y-shaped structures that mimic the shape of antibodies for better interaction with cells through the branched extensions.[10] In addition to geometry, the amino acid composition can determine the intended or unintended consequences of a peptide in bio-applications. Polar amino acids such as asparagine and glutamine, for example, can produce insoluble amyloid fibrils that cause neurodegenerative diseases, ultimately due to formation of β-structures with more hydrogen bonds (compared to α-helices) in the amino acid side-chains.[11] It is important to note that different orientations of similar amino acids can have different impacts on the conformational secondary structures, causing variations in exposure to receptor binding sites. Computer-aided modeling now allows free energy-based structure optimization of peptides and predict the conformational changes in response to ligand-receptor interactions and eventual binding efficiency.

Recently, Yan et al.[10] developed a Y-shaped peptide capable of targeting legumain, an acidic cysteine endopeptidase that has recently emerged as a tumor biomarker owing to its overexpression by tumor-associated macrophages and pro-tumor M2 polarized macrophages within tumor microenvironments of a range of cancers.[12] Legumain has a very high specificity for hydrolysis of asparaginyl bonds after the P1 site (Asn) of the substrates, and this can be used for targeting. Synthesized intracellularly as prolegumain (56 kDa), legumain auto-activates at acidic pH to an intermediate (46/47 kDa) form, which undergoes further cleavage to the mature active legumain (36 kDa).[13] The latter is recognized by a legumain antibody included in the targeting formulation. The Y-shaped legumain-targeting peptide ("Y-Leg"[10]) comprises an alanine (Ala) – asparagine (Asn) – leucine (Leu) 'targeting' linear (unbranched) segment and a branched histidine (His) – lysine (Lys) 'non-targeting' segment. Lys in the non-targeting segment allows further functionalization with entities such as nanoparticles, while His, thanks to its partially protonated imidazole side chain, affords pH-specific (pH = 5.4–6.5) interactions. Through in vitro and in vivo studies, Yan et al.[10] deduced that Y-leg, by conjugating the branched segment ('two-feet') to nanoparticles, orients the targeting segment for highly favorable and efficient interaction with legumain overexpressed in tumor microenvironments, providing a highly promising ligand for tumor nanotheranostics.
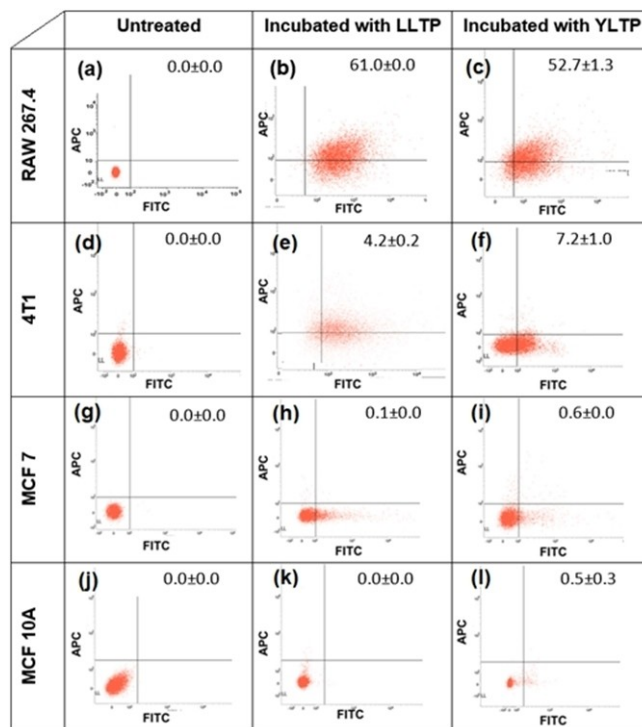
Figure 1. Flow cytometry analysis of legumain-targeting efficiency of LLTP and YLTP towards RAW 264.7, 4T1, MCF 7 and MCF 10 A cells. The percentage of cells in the "double positive" is shown on top in (a)–(l).
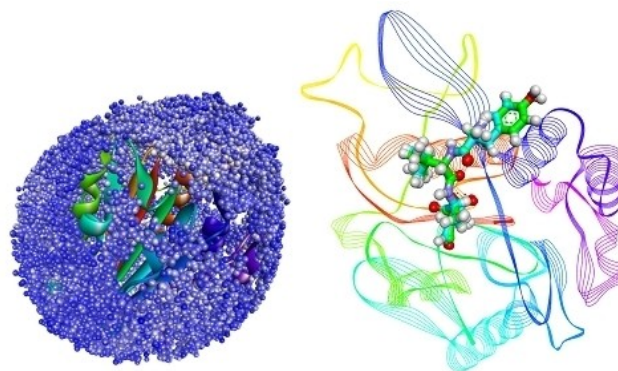
Figure 2. Left: All identified hotspots using blind docking approach. Right: Orientation of cocrystal peptide, YVAD-CMK, and redocked pose of topmost hit within the legumain protein. Cocrystal peptide is shown in green ball-and-stick while the redocked one is shown in cyan colored ball-and-stick representation.

We investigated using in vitro and in silico methodologies two geometrically different peptides with the same amino acid sequences à la Y-leg – a Y-shaped peptide and a linear unbranched peptide (see Figure S1) – for their legumain-targeting affinity. We refer to the two peptides as linear legumain-targeting peptide (LLTP) and Y-shaped legumain-targeting peptide (YLTP). In vitro cell line studies were conducted using flow cytometry and confocal fluorescence microscopy to determine the relative legumain-targeting

ChemistrySelect

Full Papers
doi.org/10.1002/slct.202002161

Chemistry
Europe
European Chemical
Societies Publishing
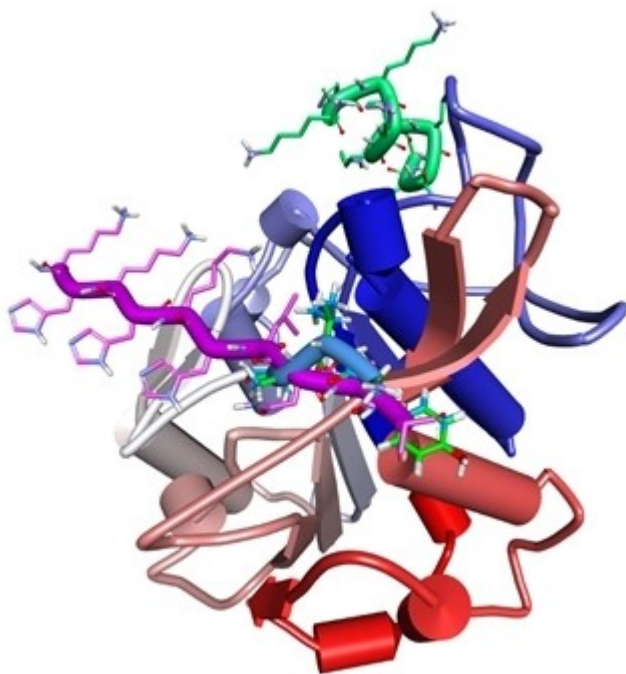
Figure 3. Binding orientation of docked cocrystal peptide (light blue), LLTP (purple), and YLTP (dark green) with legumain.
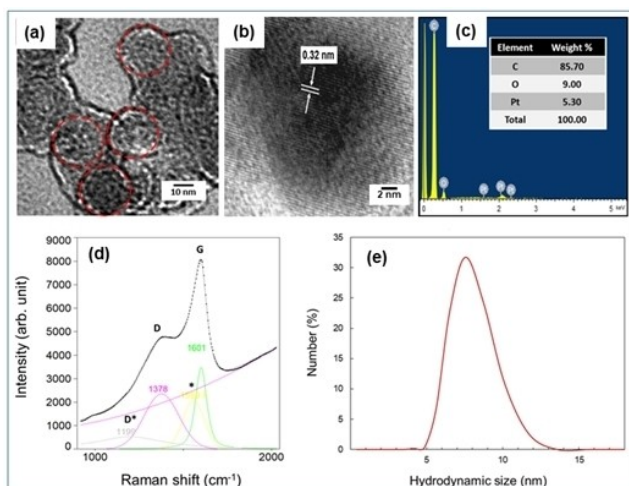
Figure 4. Characteristics of the CDs. (a) Electron micrograph of CD aggregates. (b) HRTEM image of lattice fringes. (c) EDX analysis. (d) Raman spectrum showing the D and G bands. (e) Hydrodynamic size distribution.

efficiency of the two peptides. Subsequently, molecular modeling was used to gain a deeper, structure-level understanding of the legumain binding affinity of the two peptides. The LLTP, the better performing of the two peptides, was then conjugated with CDs as a cellular imaging vector and further in vitro studies and stability assessments were carried out to reveal the bioimaging potential of the formulation. CDs are widely investigated for bio-applications including cellular imaging owing to their excellent biomaterial attributes such as ease of synthesis, tunable photoluminescence, photostability,
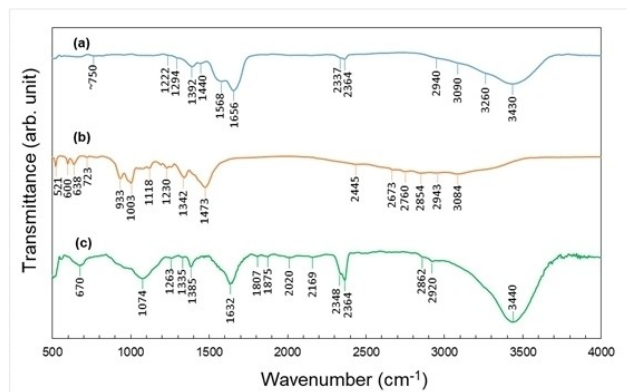
Figure 5. FTIR spectrum of CDs (a), LLTP (b), and LLTP-CDs conjugate (c).
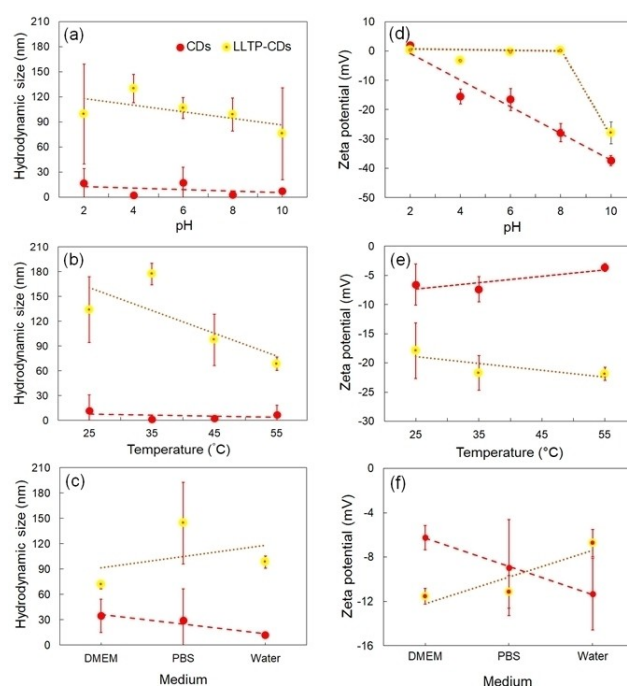
Figure 6. Hydrodynamic size and zeta potential of the CDs and the LLTP-CDs nanoparticles as a function of pH, temperature, and medium composition. Trend lines are shown as guide to the eye.

biocompatibility, noncytotoxicity, rapid clearance, excellent solubility and stability in aqueous media.[14]

Results and Discussion

Legumain-targeting efficiency of LLTP and YLTP: experimental results

Flow cytometry was used to quantify the targeting efficiency of the two geometrically different peptides towards legumain in four cell types: three tumor cells, namely, RAW 264.7 (ATCC® TIB-71™), 4T1 (ATCC® CRL-2539™), and MCF 7 (ATCC® HTB-22™); and the fourth, the non-malignant MCF 10 A (ATCC® CRL-10317™). The legumain activity on the cells was recog-

ChemistrySelect

Full Papers
doi.org/10.1002/slct.202002161

Chemistry Europe
European Chemical
Societies Publishing
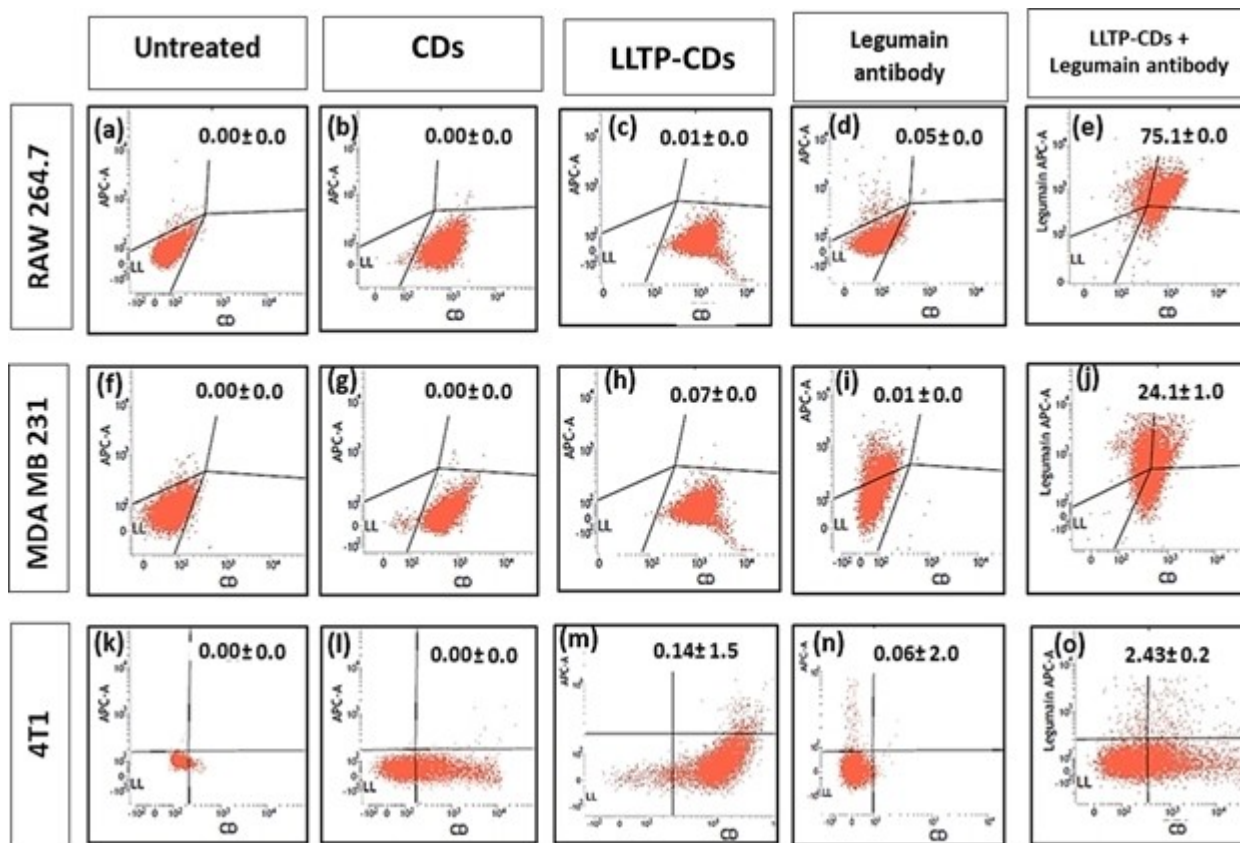
Figure 7. Cell population distributions for unstained cells [(a), (f), and (k)] and cells treated with CDs [(b), (g), and (l)], LLTP-CDs [(c), (h), and (m)], legumain antibody [(d), (i), and (n)], and both LLTP-CDs and legumain antibody [(e), (j), and (o)]. The percentage "double positive" population is shown on the top of each subpanel.

nized using fluorescence from allophycocyanin (APC) while fluorescein isothiocyanate (FITC) fluorescence signal allowed recognition of peptide binding. Binding of the peptide at the carboxyl-bonded asparaginyl site activates legumain at acidic pH of ∼5.4–6.5. The active form of legumain is bound by an anti-legumain primary antibody that has high specificity towards activated legumain. The anti-legumain primary antibody binding to legumain on the cell surface is detected using an APC-tagged secondary antibody.

The flow cytometry results are presented in Figure 1. The upper right ("double positive") quadrant in each subpanel (a)–(l) represents the cell population recording both FITC and APC fluorescence events, in effect, the legumain-targeting efficiency of the peptide. The unstained cells [Figure 1 (a), (d), (g), and (j)] act as negative control, and clearly do not show significant FITC and APC fluorescence counts. Upon treating with the LLTP, double positive binding was recorded at 61.0%, 4.2%, 0.1% and 0.0%, respectively for RAW 264.7, 4T1, MCF 7, and MCF 10 A cells [Figure 1 (b), (e), (h) and (k)]. In comparison, the YLTP-treated cells yielded double positive population of 52.7%, 7.2%, 0.6% and 0.5%, respectively for RAW 264.7, 4T1, MCF 7, and MCF 10 A cells [Figure 1 (c), (f), (i) and (l)]. Both peptides show good targeting efficiency towards RAW 264.7 cells which are known to have high expression of legumain.[15] In contrast,

the very low to almost absent double positive populations for 4T1, MCF 7, and MCF 10 A cells suggest very low legumain expression on these cells. (The slightly higher targeting by the YLTP in the latter three cell types may be considered of no significance from a bioimaging perspective.) These findings are in excellent agreement with previous studies that reported low legumain expression by these cells in culture.[16] The extremely low legumain expression by the 4T1, MCF 7, and MCF 10 A cells in culture may be explained by the fact that legumain being a stress-induced protein, its expression is influenced by cytokines produced in real tumor microenvironments[15a] It was shown that the legumain activity in culture 4T1 cells was one-third when compared to that in solid tumors induced in a mouse model following inoculation with the 4T1 cells.[13b] To summarize, the LLTP shows relatively higher targeting efficiency compared to the YLTP in legumain expressing cells such as RAW 264.7 macrophages.

The legumain-targeting affinity of the two peptides was further investigated qualitatively using fluorescence microscopy on peptide-treated RAW 264.7, 4T1, and MDA MB 231 (ATCC® HTB-26™) cells with 4',6-diamidino-2-phenylindole (DAPI) and APC as fluorochromes. The fluorescence from the cells conform to the flow cytometry results: the maximum red fluorescence is observed for RAW 264.7 cells followed by
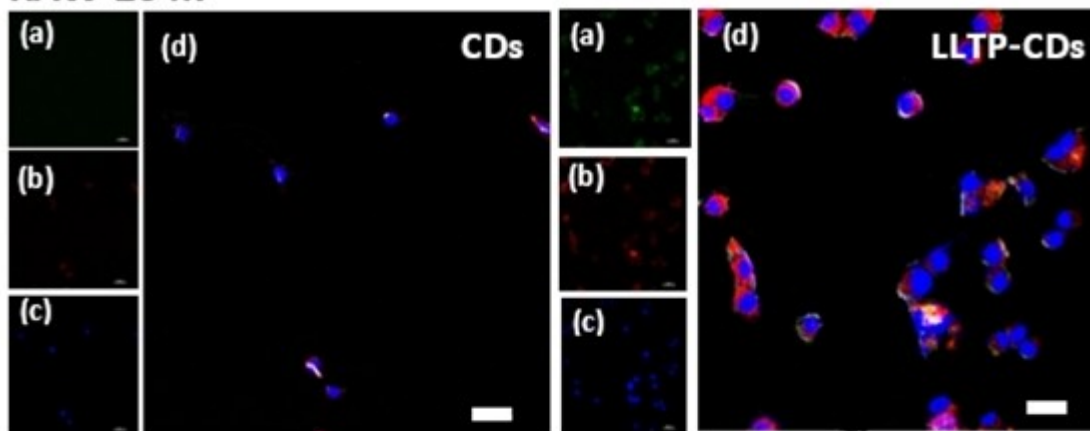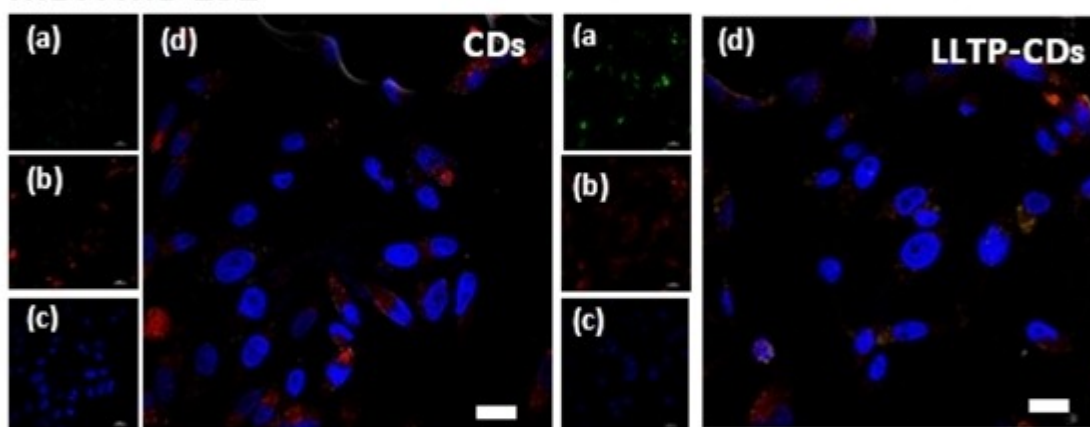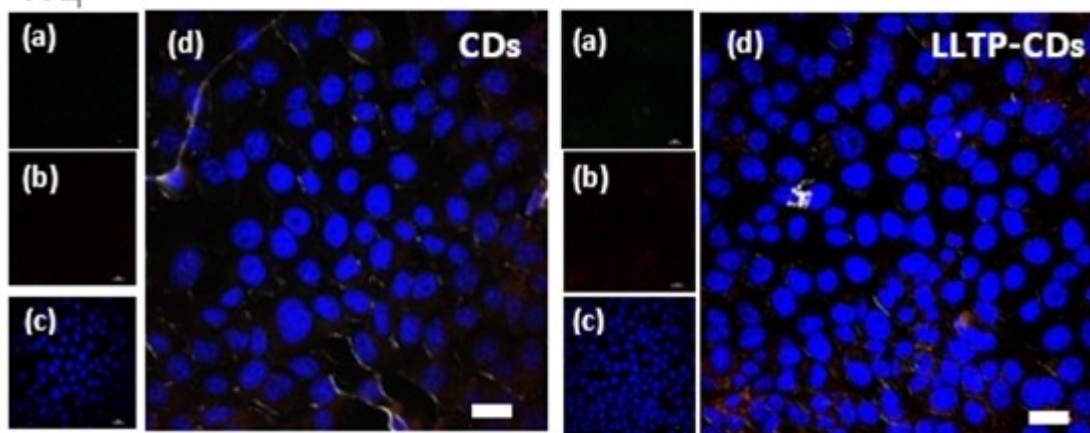
Figure 8. Fluorescence microscopy images showing cellular association of the CDs and the LLTP-CDs with RAW 264.7, MDA MB 231, and 4T1 cells. (a) Fluorescence from the CDs excited by a green laser ($\lambda = 488$ nm). (b) Fluorescence from the CDs excited by a red laser ($\lambda = 638$ nm). (c) Fluorescence from DAPI excited by UV laser ($\lambda = 325$ nm) showing cell nuclei. (d) Merged image. Scale bar: 20 μm.

moderate fluorescence from MDA MB 231 cells, and no fluorescence from 4T1 cells (Figure S2). The lower fluorescence observed for MDA MB 231 cells suggests lower legumain activity, in agreement with previous work.[17] The red APC

fluorescence is denser in the LLTP treated cells compared to that in the YLTP treated cells. Our flow cytometry and fluorescence microscopy data thus confirm that the LLTP has a higher legumain binding affinity compared to the YLTP, though

ChemistrySelect

Full Papers
doi.org/10.1002/slct.202002161

Chemistry Europe
European Chemical
Societies Publishing

we anticipated the YLTP to yield higher binding efficiency on the basis of the proposed structurally dictated binding model.[10] In order to gain a deeper, structure-level understanding of the legumain-targeting affinity of the two peptides, we carried out computational modeling of the peptide structures and peptide-legumain docking using forcefield approaches.

Peptide geometry and peptide-legumain docking from molecular modeling

Peptide-protein docking results obtained using ZDOCK and RDOCK approaches[18] are discussed below. ZDOCK seeks to identify molecular surface complementarity by efficiently exploring the six degrees of translational and rotational freedom using the fast Fourier transform technique whilst RDOCK refinement is based on CHARMM energy minimization and a re-ranking of the predicted poses using a free energy scoring function composed of electrostatic energy and desolvation energy calculated by the atomic contact energy method.[19]

Redocking of cocrystal peptide identified consistent binding pocket within the top cluster and topmost hits result.[12d] RMSD value between cocrystal and redock peptide was 0.189 Å (Figure 2). Binding orientation was also consistent with the crystallized equivalent, validating our docking protocol (Table S1).

In the absence of crystal structure data for the LLTP and the YLTP complex with legumain that would reveal detailed contact residues, we used a docking procedure to compare legumain binding to the two peptides. For each peptide, the top-ranked poses form clusters that reveal the stable binding mode and were analyzed (Figure 3). Among the docked poses in the cluster, the residues in the binding loop region of the peptide tend to exhibit much smaller backbone RMSD values than regions in the rest of the molecule. Although protein sidechain movements among the binding interface residues were observed after the RDOCK refinement, the backbone conformation changes were minor. Among the three peptides tested (cocrystal 4mer peptide, LLTP and YLTP), the LLTP comes out as the most stable form (Table S2) with the lowest minimized energy or E_RDOCK value (-20.44 kcal mol^{-1}), followed by YLTP (-18.05 kcal mol^{-1}) and redocked cocrystal (-17.39 kcal mol^{-1}). The largest negative E_RDOCK value obtained for the LLTP indicates its relatively stronger interaction with the protein compared to the other two.

Interestingly, for the legumain-LLTP complex, the top ranked amongst the 100 RDOCK predicted poses are clustered around a common binding mode, the active site of legumain. Also, the LLTP shows similar binding orientation to the cocrystal peptide, at legumain's active site (Figure 3). This finding for the legumain-LLTP complex is consistent with x-ray crystallographic data for the cocrystal (YVAD_CMK) complex with legumain. Moreover, the LLTP has the highest ZDOCK score of 9.54 (Table S2) and the highest binding affinity towards the legumain active site.

For the legumain-YLTP complex, top eight ranked of the 100 RDOCK predicted poses show similar clustering. The most

stable orientation of the YLTP with higher negative ZDOCK score was found to be at a different location to the binding location of the cocrystal peptide and LLTP. This can be explained by the change in shape of the YLTP in its most stable configuration with its asparaginyl legumain binding site (-Asn-) coiled into an α-helix form. This modification may reduce access for the peptide's binding site to the legumain active site. The experimentally observed lower legumain targeting efficiency of the YLTP may reflect the altered conformation of the stable YLTP structure.

Several intermolecular hydrogen bonds consistently formed between peptide and legumain in the peptide-legumain complex (Figures S3 and S4). The LLTP amino acids formed eight hydrogen bond interactions with legumain: three at Lys-3, one at His-4, two at His-6, and one each at Asn-8 and Ala-10. In contrast, the YLTP amino acids formed only five hydrogen bond interactions with legumain: one at His-4, two at Asn-8, and two at Ala-9. Thus, the LLTP-legumain complex with more hydrogen bonded interactions is more stable compared to the YLTP-legumain complex, consistent with the E_RDOCK values (Table S2).

The docking simulations provide a quantitative energetic picture that supports the experimental results: relatively stronger legumain-binding affinity of the LLTP. Moreover, the docking results revealed that the backbone geometry is not significantly changed in the complex. For a fuller picture of binding, structural flexibility of the two peptides, as may be revealed in a molecular dynamics simulation, is necessary. Although the docking results are suggestive only in the absence of crystal structure data, they are consistent with data for the cocrystal peptide–protein complex, stressing the role of anchor and latch residues acting in conjunction with a weakly bound, native like conformation in the formation of high affinity complexes.[20] Our further in vitro studies were performed using the better-performing LLTP (without FITC) in combination with fluorescent CDs for cellular imaging.

Characteristics of the as-synthesized CDs and the LLTP-CDs conjugate

The CD nanoparticles[23] appeared as circular aggregates under the electron microscope (Figure 4(a)) and lattice fringes with an interplanar spacing of 0.32 nm (Figure 4(b)), corresponding to the (002) crystallographic plane of graphite (JCPDS card 75–1621), were observed at high resolution. The predominant hydrodynamic diameter of the CDs is ∼7.5 nm (Figure 4(e)). The zeta potential measured for the CDs is -15.5 ± 6.3 mV, indicative of the presence of negatively charged functional groups (e.g., carboxyl).[21] Figure 4(d) shows the characteristic Raman spectral region of the CDs deconvoluted into D, D*, *, and G components following Dervishi et al.[22] The disorder-induced D band and the in-plane C–C deformational G band are around 1378 cm^{-1} and 1600 cm^{-1}, respectively. The EDX analysis of CDs (Figure 4(c)) shows carbon (85.7%), oxygen (9%), and minor Pt (from the coating). It can be concluded from the above that graphitic CDs with an average diameter of 7.5 nm was successfully synthesized.

ChemistrySelect

Full Papers
doi.org/10.1002/slct.202002161

**Chemistry
Europe**
European Chemical
Societies Publishing

The LLTP-CDs nanoparticles obtained using the microwave method[23] have average size of ~120 nm and contain significant amount of N in addition to C and O, contributed by the peptide amino groups (Figure S6). The LLTP-CDs nanoparticles yield zeta potential value of -21.8 ± 0.9 mV, indicating presence of negatively charged surface functional groups.

The FTIR spectra shown in Figure 5 indicate the molecular vibrational responses of various functional groups present in the CDs, the LLTP, and the LLTP-CDs conjugate. The CDs show FTIR bands due to O—H stretching, N—H stretching (3430 cm^{-1}, 3260 cm^{-1} and 3090 cm^{-1}), C—H stretching (~2940 cm^{-1}), —C=O stretching (~1650 cm^{-1}), C—O stretching/C—H bending (1392 cm^{-1}), and C—OH stretching (1222 cm^{-1})[24] [Figure 5(a)]. The 1568 cm^{-1} and ~700 cm^{-1} bands correspond to N—H or —NH$_2$ bending vibrations in the amide bond. Thus, the FTIR spectrum indicates hydroxyl, amino, and possibly carboxyl (although the characteristic carboxylic bands around 1710 cm^{-1} and 1150 cm^{-1} are not obvious) groups on the CDs.

The spectrum of the LLTP (Figure 5(b)) shows the characteristic amide I, amide II, and amide III bands. The bands due to N—H vibrations (933 cm^{-1}), C—O stretching (1003 cm^{-1}), N—H bending (1118 cm^{-1}), C—N stretching (1230 cm^{-1}), C—H and N—H vibrations (1342 cm^{-1}), and C—O bending of carboxylic groups (1473 cm^{-1}) are observed.[24] The FTIR spectrum of the LLTP-CDs conjugate (Figure 5(c)) appears as a combination of the other two. The asymmetric/symmetric stretching modes of the methylene group are clearly seen at 2920 cm^{-1} and 2862 cm^{-1}. N—H bending and C—N stretching (1074-1382 cm^{-1}), and C=O stretching (1600-1700 cm^{-1}) bands of amide I, and C—N stretching and N—H bending of amide II (1550-1632 cm^{-1}) are seen.[23] The new band at 1074 cm^{-1} (C—O stretching) appears to be due to the conjugation of LLTP and CDs. The significant intensity enhancements of the bands around 1000–1200 cm^{-1} and ~700 cm^{-1} may suggest covalent bonding between the CDs and the LLTP, as CDs are known to adsorb macromolecules (proteins, polysaccharides) through electrostatic or π–π bonds.

The synthesis parameters and physical/chemical nature of the CDs significantly affect the optical properties.[14] The reactant ratio, reaction temperature, particle size, oxygen content (for example, attached COOH group), etc determine the UV-visible light absorption and photoluminescence (PL) characteristics.[25] An UV-visible light absorption maximum ~330 nm with a tail towards the blue-green region was observed for the CDs (Figure S7), similar to that reported for 7–11 nm graphene dots[14c] and ~360 nm peak for CA-derived ~15 nm CDs,[25b] possibly suggesting size-dependent redshift of the absorption maximum. This absorption peak is commonly assigned to energy absorbed in the n–π* electron transition of the conjugated C—O or C—N group.[25] The absorption maximum shifts to ~340 nm for the LLTP-CDs conjugate (Figure S7). The useful PL of the CDs and LLTP-CDs conjugate is clearly seen in our PL/fluorescence data (Figure S7).

Stability of the CDs and the LLTP-CDs nanoparticles

The stability of the nanoparticles was studied by monitoring the hydrodynamic size and zeta potential under various medium composition, pH, and temperature conditions relevant to bioimaging (Figure 6). The hydrodynamic size of the CDs is not significantly affected by varying pH, temperature, and medium composition. However, the zeta potential value of the CDs is sensitive to varying pH: decreasing steadily with increasing pH. The zeta potential is also sensitive to medium composition, but less sensitive to temperature variation. This is understandable in that variations in the pH and medium composition can result in direct chemical modifications of the surface functional groups via protonation/deprotonation or other possible reactions.[26]

The hydrodynamic size of the LLTP-CDs nanoparticles decreases slightly with increase in pH and temperature (Figure 6). The zeta potential value of the LLTP-CDs conjugate is nearly constant across the temperature range and in the pH range of 2–8. The more negative zeta potential at pH > 8 suggests deprotonation of the amino group.[24a] Medium composition has a small effect on the zeta potential of the conjugate, suggesting possible chemical interactions between the CD-peptide functional groups and the medium. Overall, the nanoparticles appear stable under conditions relevant to bioimaging.

Knowledge of the optical properties under relevant pH conditions is a prerequisite for use of fluorescent nanomaterials as bioimaging agents. We have, therefore, briefly explored the effect of pH on the UV-visible light absorption and bandgap energies of the as-prepared and functionalized CDs. Published work largely examined the pH effect on PL. A small number of investigations have focused on the UV-visible light absorption, reporting contradictory results: some suggested significant pH dependence on the absorption[26,27] while others observing virtually no pH dependence.[28] Our data suggest a consistent blueshift of the absorption maximum with increasing pH (Figure S8), similar to recently reported results.[27c] The calculated bandgap energy values increase, correspondingly, with increasing pH (Figure S8). Our bandgap energies are comparable to published data.[14c] In CDs with hydroxyl and carboxylic surface functional groups, the pH-dependent light absorption has been attributed to deprotonation of the functional groups.[26] Our interest here is not concerned with the reasons for this behavior, rather to demonstrate that the nanoparticle formulations with the observed optical property reliability and physical stability under physiologically relevant pH, temperature, and medium composition conditions can be used for efficient bioimaging.

Legumain-targeting efficiency of the LLTP-CDs conjugate

Flow cytometry data on the legumain-binding efficiency of the LLTP-CDs formulation in RAW 264.7, MDA MB 231, and 4T1 cells are shown in Figure 7. Untreated cells and cells treated with CDs, LLTP-CDs, legumain antibody (negative control), and both LLTP-CDs and legumain antibody are included. The zero or

ChemistrySelect

Full Papers
doi.org/10.1002/slct.202002161

Chemistry Europe
European Chemical
Societies Publishing

near-zero double positive population suggests absence of legumain-targeting in the control samples and virtually no targeting in cells incubated with only CDs, LLTP-CDs particles, or legumain antibody. By contrast, RAW 264.7 cells treated with both LLTP-CDs and legumain-antibody show exceptionally high targeting ($75.1 \pm 1\%$) while similarly treated MDA MB 231 cells suggest moderate targeting ($24.1 \pm 1\%$) and 4T1 cells recording very low targeting ($2.43 \pm 0.2\%$). The LLTP-CDs nanoparticles appear to present higher peptide concentration to the cells compared to unconjugated LLTP (*cf.* Figure 1). The fluorescence microscopy images of the above three cell types treated with the CDs or the LLTP-CDs conjugate and stained with DAPI (Figure 8) corroborate the flow cytometry results: the highest level of fluorescence in RAW 264.7 cells, followed by MDA MB 231 cells, and very low fluorescence in 4T1 cells. Thus, the fluorescence distribution is consistent with the legumain expression levels in the cell types, and suggest a high bioimaging potential for the LLTP-CDs formulation in legumain-expressing cells.

Conclusion

Flow cytometry and fluorescence microscopy of peptide-treated RAW 264.7, 4T1, MCF 10 A, MCF 7 and MDA MB 231 cells revealed that the LLTP has a higher legumain binding efficiency compared to the YLTP in legumain-active cell types. Computational structure optimization of LLTP, YLTP, and a 4mer cocrystal peptide suggested that a linear LLTP is the most stable of the three, while the stable YLTP configuration has its asparaginyl binding site (-Asn-) coiled into an α-helix form. Peptide-legumain docking simulations revealed that the LLTP and the cocrystal peptide have similar binding orientation, both binding at legumain's active site with a higher binding affinity for the former. The YLTP-legumain binding occurs at a different site due to the coiled shape of the asparaginyl binding site in YLTP, and this possibly explains its lower experimentally observed targeting efficiency. Moreover, higher hydrogen bonding between the LLTP amino acids and legumain compared to that between the YLTP amino acids and legumain leads to a more stable LLTP-legumain conjugation. Flow cytometry and fluorescence imaging of the LLTP-CDs nanoparticles treated cell lines revealed enhanced binding efficiency of the conjugate nanoparticles towards legumain, the cellular targeting being proportional to the legumain expression level in the different cell types. We recommend the LLTP as an efficient legumain-targeting ligand for use in conjunction with a suitable fluorochrome such as CDs for bioimaging in legumain-expressing cells.

Supporting Information Summary

The experimental and computational methods are detailed in the Supporting Information. These include commercial materials used and materials synthesized and their characterization, in vitro methods (cell culture, flow cytometry, fluorescence microscopy), stability studies, and details of the computational studies concerning peptide stability and peptide-legumain

docking. In addition, the chemical structures of the peptides, fluorescence microscopy images of the peptide-treated cell types, TEM images and optical properties of the synthesized CDs and peptide-CDs conjugate, and ball-and-spoke models of peptide-legumain complexes are included in Supporting Information.

Conflict of Interest

The authors declare no conflict of interest.

[1] a) A. B. Chinen, C. M. Guan, J. R. Ferrer, S. N. Barnaby, T. J. Merkel, C. A. Mirkin, *Chem. Rev.* **2015**, *115*, 10530–10574; b) M. Ferreira, P. Almeida, M. A. Shahbazi, A. Correia, H. A. Santos, *Biomedical Chemistry: Current Trends and Developments* (Ed. N. Vale), Walter de Gruyter GmbH & Co KG: Warsaw/Berlin, **2015**, p. 361.

[2] S. R. Krishnan, S. K. George, *Pharmacology and Therapeutics* (Ed. S. J. Thatha), Gowder, IntechOpen **2014**, DOI: 10.5772/58419.

[3] a) L. D. Field, J. B. Delehanty, Y. Chen, I. L. Medintz, *Acc. Chem. Res.* **2015**, *48*,1380–1390; b) A. Komin, L. M. Russell, K. A. Hristova, P. C. Searson, *Adv. Drug Delivery Rev.* **2017**, *110–111*, 52–64; c) X. Sun, Y. Li, T. Liu, Z. Li, X. Zhang, X. Chen, *Adv. Drug Delivery Rev.* **2017**, *110–111*, 38–51; d) C. D. Spicer, C. Jumeaux, B. Gupta, M. M. Stevens, *Chem. Soc. Rev.* **2018**, *47*, 3574–3620; e) J. L. Paris, G. Villaverde, S. Gómez-Graña, M. Vallet-Regía, *Acta Biomater.* **2020**, *101*, 459–468; f) R. W. Liu, X. C. Li, W. W. Xiao, K. S. Lam, *Adv. Drug Delivery Rev.* **2017**, *110*, 13–37; g) J. S. Kanathasan, V. Swamy, U. D. Palanisamy, A. K. Radhakrishnan, *Adv Sci. Tech*, **2017**, *102*, 45–50.

[4] a) L. Zhang, A. Gülses, N. J. Purcz, J. Weimer, J. Wiltfang, Y. Açil, *Clin. Transl. Oncol.* **2019**, 1–9; b) H. L. Xin, X. Y. Jiang, J. J. Gu, X. Y. Sha, L. C. Chen, K. Law, Y. Z. Chen, X. Wang, Y. Jiang, X. L. Fang, *Biomater.* **2011**, *32*, 4293–4305.

[5] a) M. E. Davis, Z Chen, D. M. Shin, *Nat. Rev. Drug Discovery* **2008**, *7*, 771–782; b) J. J. Shi, P. W. Kantoff, R. Wooster, O. C. Farokhzad, *Nat. Rev. Cancer* **2017**, *17*, 20–37.

[6] a) K. W. Beekman, A. D. Colevas, K. Cooney, R. DiPaola, R. L. Dunn, M. Gross, E. T. Keller, K. J. Pienta, C. J. Ryan, D. Smith, M. Hussain, *Clin. Genitourin Cancer* **2006**, *4*, 299–302; b) J. Temsamani, P. Vidal, *Drug Discovery Today* **2004**, *9*, 1012–1019.

[7] a) J. Cutrera, D. Dibra, X. Q. Xia, A. Hasan, S Reed, S. L. Li, *Mol. Ther.* **2011**, *19*, 1468–1477; b) R. M. J. Liskamp, D. T. S. Rijkers, S. E. Bakker, *Modern Supramolecular Chemistry: Strategies for Macrocycle Synthesis* (Eds.: F. Diederich, P. J. Stang, R. R. Tykwinski), Wiley-VCH, Weinheim, **2008**, pp. 1–28.

[8] a) C. Wiesmann, H. W. Christinger, A. G. Cochran, B. C. Cunningham, W. J. Fairbrother, C. J. Keenan, G. Meng, A. M. de Vos, *Biochemistry* **1998**, *37*, 17765–17772; b) E. Vivès, J. Schmidt, A. Pèlegrin, *Biochim. Biophys. Acta* **2008**, *1786*, 126–138.

[9] a) M. Lee, B. Gardner, M. Kahn, H. Nakanishi, *FEBS Lett.* **1995**, *359*, 113–118; b) A. Roxin, G. Zheng, *Future Med. Chem.* **2012**, *4*, 1601–18.

[10] L. Yan, Y. X. Gao, R. Pierce, L. M. Dai, J. Kim, M. Zhang, *Mater. Res. Express* **2014**, *1*, 1–14.

[11] a) Y. Zhang, V. H. Man, C. Roland, C. Sagui, *ACS Chem. Neurosci.* **2016**, *7*, 576–587; b) K. J. Wolfe, D. M. Cyr, *Semin. Cell Dev. Biol.* **2011**, *22*, 476–481.

ChemistrySelect

Full Papers
doi.org/10.1002/slct.202002161

**Chemistry
Europe**
European Chemical
Societies Publishing

[12] a) E. Dall, H. Brandstetter, *Biochimie* **2016**, *122*, 126–150; b) J. M. Chen, P. M. Dando, N. D. Rawlings, M. A. Brown, N. E. Young, R. A. Stevens, E. Hewitt, C. Watts, A. J. Barrett, *J. Biol. Chem.* **1997**, *272*, 8090–8098; c) J. M. Chen, P. M. Dando, R. A. E. Stevens, M. Fortunato, A. J. Barrett, *Biochem. J.* **1998**, *335*,111–117; d) E. Dall, H. Brandstetter, *Proc. Natl. Acad. Sci. USA* **2013**, *110*, 10940–10945.

[13] a) D. N. Li, S. P. Matthews, A. N. Antoniou, D. Mazzeo, C. Watts, *J. Biol. Chem.* **2003**, *278*, 38980–38990; b) K. M. Bajjuri, Y. Liu, C. Liu, S. C. Sinha, *ChemMedChem* **2011**, *6*, 54–59.

[14] a) L. Cao, X. Wang, M. J. Meziani, F. Lu, H. Wang, P. G. Luo, Y. Lin, B. A. Harruff, L. Monica Veca, D. Murray, S. Y. Xie, Y. P. Sun, *J. Am. Chem. Soc.* **2007**, *129*, 11318–11319; b) S. Chandra, P. Das, S. Bag, D. Laha, P. Pramanik, *Nanoscale* **2011**, *3*, 1533–1540; c) J. Peng, W. Gao, B. K. Gupta, Z. Liu, R. Romero-Aburto, L. Ge, L. Song, L. B. Alemany, X. Zhan, G. Gao, S. A. Vithayathil, B. A. Kaipparettu, A. A. Marti, T. Hayashi, J. J. Zhu, P. M. Ajayan, *Nano Lett.* **2012**, *12*, 844–849.

[15] a) L. E. Edgington, M. Verdoes, A. Ortega, N. P. Withana, J. Lee, S. Syed, M. H. Bachmann, G. Blum, M. Bogyo, *J. Am. Chem. Soc.* **2013**, *135*, 174–182; b) J. Lee, M. Bogyo, *ACS Chem. Biol.* **2009**, *5*, 233–243; c) Y. Luo, H. Zhou, J. Krueger, C. Kaplan, S. H. Lee, C. Dolman, D. Markowitz, W. Wu, C. Liu, R. A. Reisfeld, R. Xiang, *J. Clin. Invest.* **2006**, *116*, 2132–2141.

[16] J. J. Briggs, M. H. Haugen, H. T. Johansen, A. I. Riker, M. Abrahamson, O. Fodstad, G. M. Maelandsmo, R. Solberg, *BMC Cancer* **2010**, *17*, 1–13.

[17] Q. Qi, O. Obianyo, Y. Du, H. Fu, S. Li, K. Ye, *J. Med. Chem.* **2017**, *60*, 7244–7255.

[18] a) R. Chen, L. Li, Z. Weng, *Proteins* **2003**, *52*, 80–87; b) L. Li, R. Chen, Z. Weng, *Proteins* **2003**, *53*, 693–707.

[19] a) E. Katchalski-Katzir, I. Shariv, M. Eisenstein, A. A. Friesem, C. Aflalo, I. A. Vakser, *Proc. Natl. Acad. Sci. USA* **1992**, *89*, 2195–2199; b) C. Zhang, G. Vasmatzis, J. L. Cornette, C. DeLisi, *J. Mol. Biol.* **1997**, *267*, 707–726.

[20] D. Rajamani, S. Thiel, S. Vajda, C. J. Camacho, *Proc. Natl. Acad. Sci. USA* **2004**, *101*, 11287–11292.

[21] S. Bhattacharyya, F. Ehrat, P. Urban, R. Teves, R. Wyrwich, M. Döblinger, J. Feldmann, A. S. Urban, J. K. Stolarczyk, *Nat. Commun.* **2017**, *8*, 1401.

[22] E. Dervishi, Z. Q. Ji, H. Htoon, M. Sykora, S. K. Doorn, *Nanoscale* **2019**, *11*, 16571–16581.

[23] The CDs were prepared from citric acid and ethylenediamine using the method by a) S. Zhu, Q. Meng, L. Wang, J. Zhang, Y. Song, H. Jin, K. Zhang, H. Sun, H. Wang, B. Yang, *Angew. Chem. Int. Ed.* **2013**, *52*, 3953–3957; The CDs appear as circular aggregates as also observed in some previous studies, for example by b) M. Bayati, J. Dai, A. Zambrana, C. Rees, M. F. Cortalezzi, *J. Environ. Sci.* **2017**, *65*, 223–235; The peptide-CDs conjugates were prepared using a modified microwave method after c) Y. Zhong, F. Peng, X. Wei, Y. Zhou, J. Wang, X. Jiang, Y. Su, S. Su, T. Lee, Y. He, *Angew. Chemie Int. Ed.* **2012**, *51*, 8485–8489.

[24] a) A. Sachdev, I. Matai, P. Gopinath, *RSC Adv.* **2014**, *4*, 20915–20921; b) M. A. Larrubia, G. Ramis, G. Busca, *Appl. Catal. B* **2000**, *27*, L145-L151.

[25] a) F. Arcudi, L. Đorđević, M. Prato, *Angew. Chemie Int. Ed.* **2017**, *56*, 4170–4173; b) Y. Dong, J. Shao, C. Chen, H. Li, R. Wang, Y. Chi, X. Lin, G. Chen, *Carbon* **2012**, *50*, 4738–4743; c) S. Chandra, A. R. Chowdhuri, D. Laha, S. K. Sahu, *Luminescence* **2018**, *33*, 336–344.

[26] S. D. Choudhury, J. M. Chethodil, P. M. Gharat, P. K. Praseetha, H. Pal, *J. Phys. Chem. Lett.* **2017**, *8*, 1389–1395.

[27] a) D. Pan, J. Zhang, Z. Li, C. Wu, X. Yan, M Wu, *Chem. Commun.* **2010**, *46*, 3681–3683; b) C. Zheng, X. An, J. Gong, *RSC Adv.* **2015**, *5*, 32319–32322; c) C. W. Lei, M. L. Hsieh, W. R. Liu, *Dyes Pigm.* **2019**, *169*, 73–80.

[28] B. Konkena, S. Vasudevan, *J. Phys. Chem. Lett.* **2014**, *5*, 1–7.